# PROOF COVER SHEET

Author(s): Jorge Belinha, Renato M. Natal Jorge, Lúcia</fnm>M.J.S.<snm>Dinis

Article title: A meshless microscale bone tissue trabecular remodelling analysis considering a new anisotropic bone tissue material law

Article no: 654783

Enclosures: 1) Query sheet
2) Article proofs

Dear Author,

**1. Please check these proofs carefully**. It is the responsibility of the corresponding author to check these and approve or amend them. A second proof is not normally provided. Taylor & Francis cannot be held responsible for uncorrected errors, even if introduced during the production process. Once your corrections have been added to the article, it will be considered ready for publication.

Please limit changes at this stage to the correction of errors. You should not make insignificant changes, improve prose style, add new material, or delete existing material at this stage. Making a large number of small, non-essential corrections can lead to errors being introduced. We therefore reserve the right not to make such corrections.

For detailed guidance on how to check your proofs, please see http://journalauthors.tandf.co.uk/production/checkingproofs.asp.

**2. Please review the table of contributors below and confirm that the first and last names are structured correctly and that the authors are listed in the correct order of contribution.** This check is to ensure that your name will appear correctly online and when the article is indexed.

| Sequence | Prefix | Given name(s) | Surname | Suffix |
|---|---|---|---|---|
| 1. | | Jorge | Belinha | |
| 2. | | Renato M. Natal | Jorge | |
| 3. | | Lúcia | M.J.S.Dinis | |

Queries are marked in the margins of the proofs.

# AUTHOR QUERIES

General query: You have warranted that you have secured the necessary written permission from the appropriate copyright owner for the reproduction of any text, illustration, or other material in your article. (Please see http://journalauthors.tandf.co.uk/preparation/permission.asp.) Please check that any required acknowledgements have been included to reflect this.

**AQ1** Please check and confirm the change made in the sentence "Like many initial anisotropic bone material laws, … bone behaviour" for clarity.

**AQ2** Please check and confirm the change made in the sentence "Using the natural neighbour concept, the NNRPIM helps … the natural behaviour of cell (Dinis et al. 2007)" for clarity.

**AQ3** Please check and confirm the change made in the sentence "The results from the work of Zioupos et al. (2008) show that the relation … but instead it is a 'boomerang'-like pattern" for clarity

**AQ4** Please check and confirm the change made in the sentence "As in the curve for the elasticity modulus in the axial direction, … are presented in Table 2" for clarity.

**AQ5** Please check and confirm the change made in the sentence "In Shefelbine et al.s work (2005), the trabecular regeneration process and cubic bone patches are analysed to verify the proposed fuzzy-logic algorithm" for clarity.

**AQ6** Please confirm whether it is [Beaupré et al. (1990a] or [Beaupré et al. (1990b].

**How to make corrections to your proofs using Adobe Acrobat**

Taylor & Francis now offer you a choice of options to help you make corrections to your proofs. Your PDF proof file has been enabled so that you can edit the proof directly using Adobe Acrobat. This is the simplest and best way for you to ensure that your corrections will be incorporated. If you wish to do this, please follow these instructions:

1. Save the file to your hard disk.

2. Check which version of Adobe Acrobat you have on your computer. You can do this by clicking on the "Help" tab, and then "About."

If Adobe Reader is not installed, you can get the latest version free from http://get.adobe.com/reader/.

- If you have Adobe Reader 8 (or a later version), go to "Tools"/ "Comments & Markup"/ "Show Comments & Markup."

- If you have Acrobat Professional 7, go to "Tools"/ "Commenting"/ "Show Commenting Toolbar."

3. Click "Text Edits." You can then select any text and delete it, replace it, or insert new text as you need to. If you need to include new sections of text, it is also possible to add a comment to the proofs. To do this, use the Sticky Note tool in the task bar. Please also see our FAQs here: http://journalauthors.tandf.co.uk/production/index.asp.

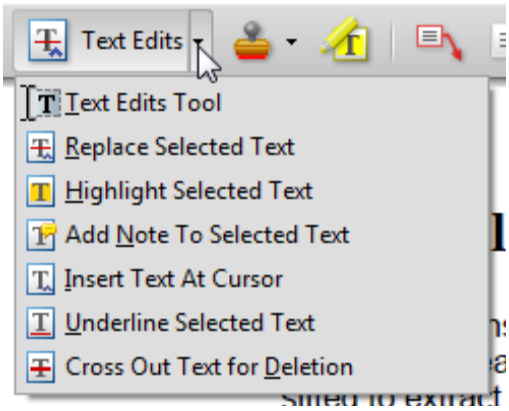


4. Make sure that you save the file when you close the document before uploading it to CATS using the "Upload File" button on the online correction form. A full list of the comments and edits you have made can be viewed by clicking on the "Comments" tab in the bottom left-hand corner of the PDF.

If you prefer, you can make your corrections using the CATS online correction form.

*Computer Methods in Biomechanics and Biomedical Engineering*
Vol. 00, No. 0, 2012, 1–15

Taylor & Francis
Taylor & Francis Group

# A meshless microscale bone tissue trabecular remodelling analysis considering a new anisotropic bone tissue material law

Jorge Belinha[a]*, Renato M. Natal Jorge[b1] and Lúcia M.J.S.Dinis[b2]

[a]*IDMEC, Institute of Mechanical Engineering, Rua Dr. Roberto Frias, 4200-465 Porto, Portugal;* [b]*Faculty of Engineering of the University of Porto (FEUP), Rua Dr. Roberto Frias, 4200-465 Porto, Portugal*

(*Received 4 July 2011; final version received 2 January 2012*)

In this work, a novel anisotropic material law for the mechanical behaviour of the bone tissue is proposed. This new law, based on experimental data, permits to correlate the bone apparent density with the obtained level of stress. Combined with the proposed material law, a biomechanical model for predicting bone density distribution was developed, based on the assumption that the bone structure is a gradually self-optimising anisotropic biological material that maximises its own structural stiffness. The strain and the stress field required in the iterative remodelling process are obtained by means of an accurate meshless method, the Natural Neighbour Radial Point Interpolation Method (NNRPIM). Comparing with other numerical approaches, the inclusion of the NNRPIM presents numerous advantages such as the high accuracy and the smoother stress and strain field distribution. The natural neighbour concept permits to impose organically the nodal connectivity and facilitates the analysis of convex boundaries and extremely irregular meshes. The viability and efficiency of the model were tested on several trabecular benchmark patch examples. The results show that the pattern of the local bone apparent density distribution and the anisotropic bone behaviour predicted by the model for the microscale analysis are in good agreement with the expected structural architecture and bone apparent density distribution.

**Keywords:** bone tissue anisotropic material law; bone remodelling; meshless method; microscale analysis

## 1. Introduction

Bone tissue is a living material, constantly responding to external and internal signals. The bone remodelling process is induced by changes in bone stress and strain fields, forcing the bone to adapt the shape and rebuild the internal microstructure.

Wolff (1986) was the first to note the relationship between the bone structure and the applied loads and to describe the adaptive capacity of the bone tissue. Since then, many theoretical and numerical models (Cowin and Hegedus 1976; Carter et al. 1987) have been developed to simulate mechanical bone mass regulation. These first works seek the minimisation of an objective remodelling function, the local strain-energy density (SED), to achieve a close relationship between the maintenance of bone mass and the local strain values in the tissues (Carter et al. 1989; Beaupré et al. 1990a; Weinans et al. 1992). In these studies, the most important variable affected by the remodelling process was the bone apparent density and the trabecular bone tissue was described as an isotropic material. However, the bone clearly shows an anisotropic behaviour. During the remodelling process, principal stress variable values and directions change locally, leading to a global anisotropic behaviour. Nonetheless, early bone models were assumed isotropic. Besides the numerical problems of anisotropic simulation of bone remodelling (Beaupré et al. 1990b; Jacobs et al. 1997), these early works had to deal with the lack of a comprehensive data bank incorporating the material properties of bone as a function of the orthotropic load directions. Therefore, several anisotropic bone material laws based on experimental studies were proposed and developed (Wirtz et al. 2000). Like many initial anisotropic bone material laws, Lotz et al. (1991) suggest distinct mathematical laws to know the cortical and trabecular bone behaviour. However, a recent experimental study (Zioupos et al. 2008) proves that the law governing the cortical and trabecular bone behaviour is in fact the same. This idea is being corroborated by the analysis of high-resolution three-dimensional images, from which some authors were able to estimate the homogenised anisotropic mechanical properties (Sansalone et al. 2010). In this work, using experimental results (Zioupos et al. 2008), a new anisotropic bone tissue material law is proposed – a new unified law to predict the cortical and trabecular bone mechanical behaviour.

A numerical method is required to obtain the stress field; in this work, a recently developed meshless method is used. Meshless methods (Nguyen et al. 2008) were created and developed to respond to some drawbacks and limitations found in the finite element method (FEM).

*Corresponding author. Email: jorge.belinha@fe.up.pt

ISSN 1025-5842 print/ISSN 1476-8259 online

http://dx.doi.org/10.1080/10255842.2012.654783
http://www.tandfonline.com

In meshless methods, the nodes can be randomly distributed as the field function is approximated within a flexible influence domain rather than an element. In opposition to the no-overlap rule between elements in the FEM, the influence domains may and must overlap each other in meshless methods.

In this work, a truly interpolator meshless method is used, i.e. the Natural Neighbour Radial Point Interpolation Method (NNRPIM) (Dinis et al. 2007). The major advantages of NNRPIM over the FEM and other meshless methods are the remeshing flexibility, the variable field higher accuracy (displacement, strain and stress fields) and the competitive computational time (Dinis et al. 2007, 2008, 2009, 2010). As the NNRPIM produces smooth and accurate stress and strain fields, high-quality SED fields are expected from this mehsless approach. Using the natural neighbour concept, the NNRPIM helps determine organically the influence domain, and therefore approaching the natural behaviour of cell (Dinis et al. 2007). This innovation on the nodal connectivity enforcement permits the analysis of convex boundaries and extremely irregular meshes, which is an advantage in the biomechanical analysis, with no extra computational effort associated. Regarding the bone tissue remodelling analysis, there are not many works on meshless methods available in the literature – the most relevant work on the subject is probably the work of Doblaré et al. (2005).

## 2. Bone tissue biomechanical model

The bone tissue is a connective tissue formed by cells, blood vessels, fibbers and organic (collagen) and inorganic substances (carbonated hydroxyapatite). However, in opposition to other connective tissues, the extracellular components suffer calcification, which confers hardness. Because of the collagen fibbers, the bone present high values for the elastic modulus and the ultimate strength in tension. In compression, the high value for the ultimate strength is given by the mineral components. At the end, the product is a light material with a microscopic and macroscopic layout, which maximises the resistance and minimises the weight. The cortical bone tissue presents a higher apparent density, and the trabecular bone tissue shows a considerably smaller apparent density. Although both types show the same molecular arrangement (microscale), the global mechanical behaviour is different (macroscale). Many experimental studies show that the bone mechanical properties depend on the bone composition and bone apparent density (Carter and Hayes 1977; Carter and Spengler 1978; Gibson 1985; Goldstein 1987; Rice et al. 1988; Martin 1991). This work proposes a new gradient remodelling approach combined with a new bone tissue anisotropic mechanical law, which only considers mechanical stimulus.

### 2.1. Material law

With the work of Lotz et al. (1991), one of the firsts to consider the bone orthotropic behaviour, it is possible to determine the elasticity modulus and the ultimate compressive stress mathematical laws for both cortical and trabecular bone in the axial and transversal directions using as variable only the apparent density, $\rho_{app}$. The macroscale bone mechanical properties are approximated with the expression:

$$\begin{cases} E_i = a_1 \cdot \left(\rho_{app}\right)^{a_2} \\ \sigma_i^c = a_3 \cdot \left(\rho_{app}\right)^{a_4} \end{cases} \quad (1)$$

where $E_i$ is the elasticity modulus and $\sigma_i^c$ is the ultimate compression stress in direction $i$, both are expressed in MPa and the apparent density $\rho_{app}$ in g/cm$^3$. The coefficients $a_j$ are presented in Table 1 in the axial and transversal directions for both cortical and trabecular bone.

Zioupos et al.'s (2008) experimental study reinforces the idea that the density is a salient property of bone and plays a crucial role in determining the mechanical properties of both its trabecular and cortical structural forms. The study, using the measured apparent density from cubic micropatches, was able to objectively isolate the bone in trabecular and compact forms. The results from the work of Zioupos et al. (2008) show that the relation between $E_i$ and the medium $\rho_{app}$ is not an increasing monotonic function, as it is in the case of Lotz et al.' (1991) law, but instead it is a 'boomerang'-like pattern. The experimental work of Zioupos et al. (2008) also shows that the law governing the mechanical behaviour of the bone tissue is the same for cortical and trabecular bone. The experimental data shown in Zioupos et al.'s (2008) work are illustrated in Figure 1(a). Thus, following the conclusions of Zioupos et al. (2008) this work proposes a unified law for cortical and trabecular bone. The bone

Table 1. Lotz law coefficients.

| Bone tissue | Direction | $a_1$ | $a_2$ | $a_3$ | $a_4$ |
|---|---|---|---|---|---|
| Cortical | Axial | 2.065E + 03 | 3.090E + 00 | 7.240E + 01 | 1.880E + 00 |
| | Transversal | 2.314E + 03 | 1.570E + 00 | 3.700E + 01 | 1.510E + 00 |
| Trabecular | Axial | 1.904E + 03 | 1.640E + 00 | 4.080E + 01 | 1.890E + 00 |
| | Transversal | 1.157E + 03 | 1.780E + 00 | 2.140E + 01 | 1.370E + 00 |

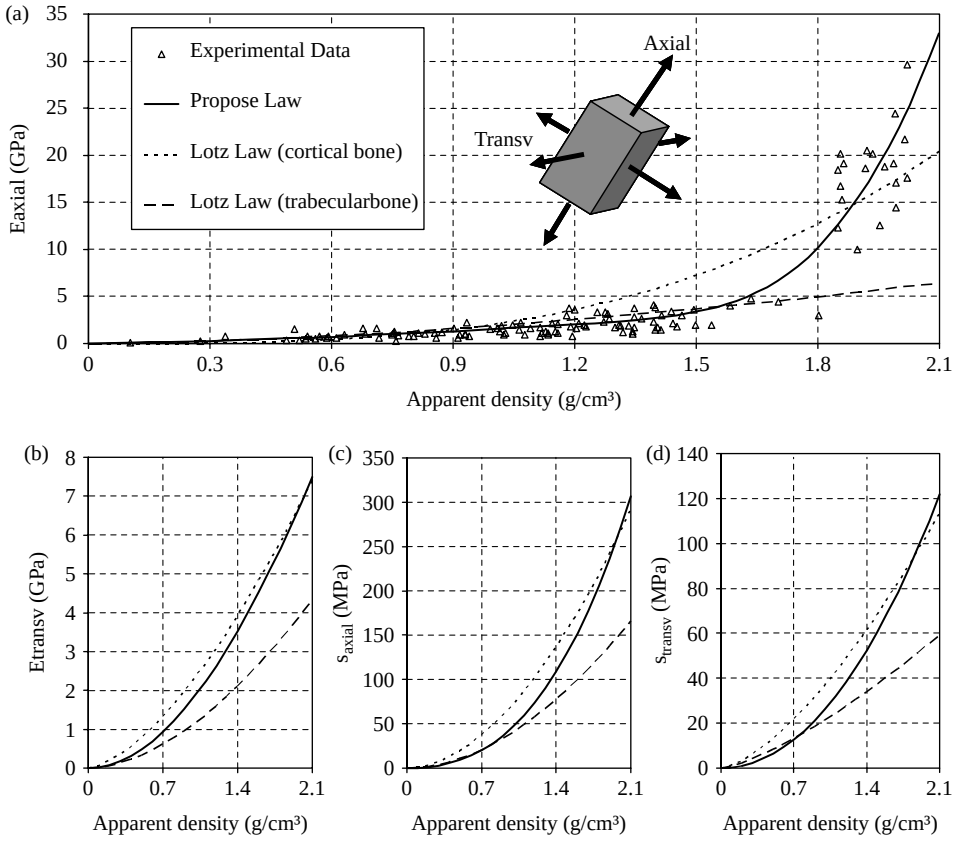


Figure 1. (a) Elasticity modulus in the axial direction. Experimental data obtain in Zioupos work compared with Lotz law for cortical and trabecular bone and with the mathematical model proposed in this work; (b) elasticity modulus in the transversal direction; (c) compression stress in the axial direction; (d) compression stress in the transversal direction.

elasticity modulus for the axial direction is obtained using the approximation curve:

$$\begin{cases} E_{\text{axial}} = \sum_{j=0}^{3} a_j \cdot (\rho_{\text{app}})^j & \text{if} \quad \rho_{\text{app}} \leq 1.3\text{g/cm}^3 \\ E_{\text{axial}} = \sum_{j=0}^{3} b_j \cdot (\rho_{\text{app}})^j & \text{if} \quad \rho_{\text{app}} > 1.3\text{g/cm}^3 \end{cases} \tag{2}$$

where the coefficients $a_j$ and $b_j$ are presented in Table 2. The proposed curve presents a 95% correlation with the experimental data (Figure 1(a)). Since in Zioupos et al.'s (2008) work only the bone elasticity modulus in the axial direction is analysed, the other curves related with the elasticity modulus in the transversal direction and the ultimate compression stress in the axial and transversal directions were obtained based on the values suggested by Lotz et al. (1991). As in the curve for the elasticity modulus in the axial direction, the other curves suggested in this work unify the cortical and trabecular bone curves:

$$\begin{cases} E_{\text{trans}} = \sum_{j=0}^{3} c_j \cdot (\rho_{\text{app}})^j \\ \sigma^c_{\text{axial}} = \sum_{j=0}^{3} d_j \cdot (\rho_{\text{app}})^j \\ \sigma^c_{\text{trans}} = \sum_{j=0}^{3} e_j \cdot (\rho_{\text{app}})^j \end{cases} \tag{3}$$

where the coefficients $c_j$, $d_j$ and $e_j$ are presented in Table 2. The elasticity modulus and the ultimate compression stress approximated by the curves presented in Equations (2) and (3) are expressed in MPa and the apparent density $\rho_{\text{app}}$ in

Table 2. Coefficients of the propose bone model.

| Coefficient | $j = 0$ | $j = 1$ | $j = 2$ | $j = 3$ |
|---|---|---|---|---|
| $a_j$ | 0.000E + 00 | 7.216E + 02 | 8.059E + 02 | 0.000E + 00 |
| $b_j$ | − 1.770E + 05 | 3.861E + 05 | − 2.798E + 05 | 6.836E + 04 |
| $c_j$ | 0.000E + 00 | 0.000E + 00 | 2.004E + 03 | − 1.442E + 02 |
| $d_j$ | 0.000E + 00 | 0.000E + 00 | 2.680E + 01 | 2.035E + 01 |
| $e_j$ | 0.000E + 00 | 0.000E + 00 | 2.501E + 01 | 1.247E + 00 |

g/cm$^3$. The plot of the approximation curve for the elasticity modulus in the transversal direction is presented in Figure 1(b), and the approximation curves for the compression stress in the axial and transversal directions are presented in Figure 1(c) and (d), respectively. The ultimate tension stress of the bone tissue is usually defined as a proportion of the ultimate compression stress, $\sigma_i^t = \alpha \cdot \sigma_i^c$. The value of $\alpha$ to be used is not consensual (Reilly and Burstein 1975; Keyak and Rossi 2000), in the various works available in the literature $\alpha$ varies between 0.33 and 1.00; therefore, in this work it will be considered $\alpha = 0.5$, once it is a conservative value.

### 2.2. *Anisotropic gradient remodelling algorithm*

The remodelling algorithm considered in the architectural optimisation analysis of bone tissue with the NNRPIM is an adaptation of Carter et al.'s (1987) remodelling algorithm. It is based on the assumption that the adaptation of bony tissue responds mainly to mechanical stimulus, acting as driving forces in the remodelling process, which can be suitably described by stress and/or strain measures. The local density and material orientation is dependent on the stress/strain field caused by the mechanical load. A forward Euler scheme is implemented, resulting in the iterative remodelling process illustrated in Figure 2.

After the pre-processing phase, the iterative remodelling algorithm is initiated. For each applied load case $i$, the strain field $\varepsilon^i$ and the stress field $\sigma^i$ are obtained. The principal stresses and directions can be obtained using the stress field $\sigma^i$. Further, the SED field for the considered load case is determined using the stress and the strain field:

$$U^i = \frac{1}{2}\sigma^T \varepsilon \tag{4}$$

With the obtained variable fields for each load cycle, the final generic variable field $\xi$ is calculated by an appropriate superposition of a number of relevant discrete load cases $l$, weighted according to the corresponding number of load cycles $m$:

$$\xi = \sum_{i=1}^{l} \frac{m_i \xi^i}{\sum_{j=1}^{l} m_j} \tag{5}$$

Afterwards the domain regions with lower SED are subject to a density remodelling process, all the other domain regions maintain the previous density. Considering the principal stress field weighted according to Equation (5), the new apparent density of the domain regions with lower SED is obtained by back substitution in Equations (2) and (3).

In the next iteration step, using the obtained new apparent density, new material properties are determined with Equations (2) and (3). Then, the material properties are oriented using the weighted principal directions obtained in the previous iteration step with Equation (5), orienting each time the material with the actualised load path. The process stops when the medium bone density reaches a controlled value. The global domain medium bone density is calculated by Equation (6):

$$\rho_{\text{app}}^{\text{med}} = \frac{1}{n}\sum_{j=1}^{n} \rho_{\text{app}}^{j} \tag{6}$$

where $n$ represents the total number of interest points and $\rho_{\text{app}}^{j}$ is the infinitesimal apparent density on interest point $j$. The used iterative process is the forward Euler scheme with the particular adaptations to suit the bone internal remodelling analysis.

The innovation of the bone tissue remodelling algorithm proposed in this work lies on the use of a new bone tissue anisotropic material law and on the smooth gradient transition of the local medium apparent density, respecting a gradient transition from the initial isotropic cortical assumption to the final anisotropic trabecular

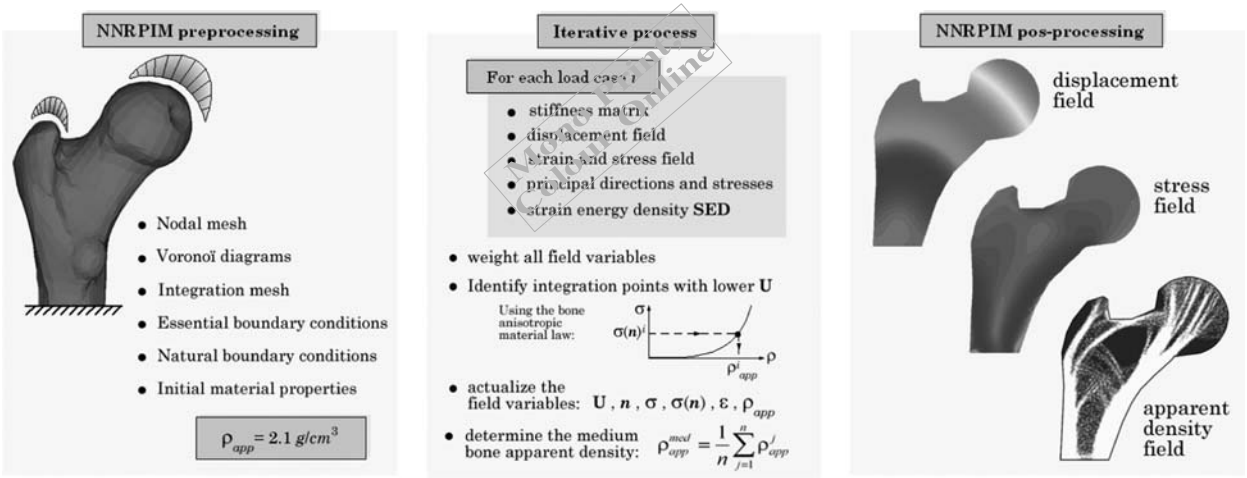


Figure 2. Proposed bone remodelling algorithm.

arrangement. The inclusion of this particular meshless method in the remodelling analysis is an asset and not just another way to obtain the stress and the strain field, as the accuracy of the remodelling algorithm depends on the accuracy of the used numerical method.

## 3. Examples

In this section, the proposed bone remodelling algorithm, using the NNRPIM, is applied to two- and three-dimensional bone micropatches (Figure 3(a)). The purpose is to validate the biomechanical numerical model, comparing the obtain solutions with available solutions in literature. Both Lotz et al.'s material law and the proposed material law are studied and compared.

In all examples, the results regarding evolution of the trabecular architecture are presented as grey tone isomaps. The analysed patch domain is discretised by a nodal mesh, and in the end of each iteration step the local apparent density, for each node, is obtained. Therefore, in the grey tone isomaps the white colour represents the considered maximum apparent density $\rho_{app}^{local} = 2.1 g/cm^3$ and the dark grey colour represents the minimum apparent density $\rho_{app}^{local} = 0.1 g/cm^3$ allowed. All other grey tones in the middle represent transitional apparent densities. Each isomap presented also indicated the patch medium apparent density, which is obtained by applying Equation (6).

### 3.1. *Two-dimensional bone patch*

In this section, the two-dimensional patch with dimensions $2 \times 2$ mm$^2$ presented in Figure 3(b) is studied. This benchmark example (Xinghua et al. 2002; Mullender et al. 1994) is used to validate the bone trabecular remodelling algorithms. The two-dimensional patch is subjected to a compressive stress distribution, decreasing linearly over the top edge. The node displacement is constrained for $y = 0$ only in the $y$ direction and in the origin is constrained in both $x$ and $y$ directions. The natural and essential boundary conditions are presented in Figure 3(b). The patch domain is discretised in the irregular nodal mesh indicated in Figure 3(c). For all studied examples, a uniformly initial density distribution $\rho_{app}^{max} = 2.1 g/cm^2$ is assumed, with a Poisson ration $\upsilon = 0.3$, regardless of the material direction. For comparison purposes, the patch was analysed using the proposed bone tissue material law and afterwards the Lotz et al.'s material law.

For decreasing patch medium apparent densities, it is possible to observe the evolution of bone tissue remodelling process for both the material laws considered (Figure 4). The results obtained with the proposed material law, Figure 4(a), are in very good agreement with the ones shown in Xinghua et al. (2002) and Mullender et al. (1994).

To validate the remodelling algorithm, when distinct mechanical load cases are considered, the bone patch was subjected to two individual loads: a load case L1 (Figure 3(b)) and a load case L2 (Figure 3(d)) – in both cases, the sample load has the same magnitude. In the first approach, load case L1 was applied with 1000 cycles and load case L2 with also 1000 cycles. Only the new anisotropic material law proposed was considered. The problem was analysed with the same mesh as in previous analysis (Figure 3(c)). The results are shown in Figure 5(a). As it was expected the trabecular remodelling resembles in both directions, $x$ and $y$.

A final test regarding the square bone patch example was conducted. The two load cases already referred were now applied with the following condition: load case L1 was applied with 1000 cycles and load case L2 with 5000 cycles. All other variables remain the same as in the previous study. The results are shown in Figure 5(b). It is clear in the trabeculae structural design preference. The trabeculae developed towards the higher load, in the $y$ direction.

Combined with the proposed new material law and the NNRPIM accuracy, the results on this benchmark example have shown the capacity of the proposed remodelling algorithm, for predicting the principal and secondary trabecular structures for the two-dimensional analysis.

### 3.2. *Three-dimensional bone patch*

In Shefelbine et al.'s work (2005), the trabecular regeneration process and cubic bone patches are analysed to verify the proposed fuzzy-logic algorithm. In the present work, similar hexahedron bone patches are studied. First, a three-dimensional patch presented in Figure 6(a) isconsidered,

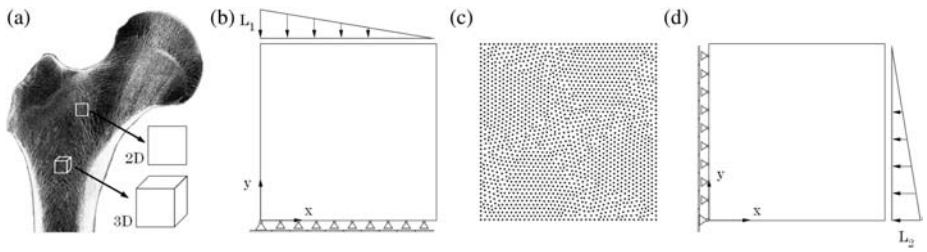


Figure 3. (a) 2D and 3D patches; (b) patch model geometry and essential and natural boundary conditions; (c) irregular nodal mesh (1952 nodes); (d) second load case considered in the analysis.

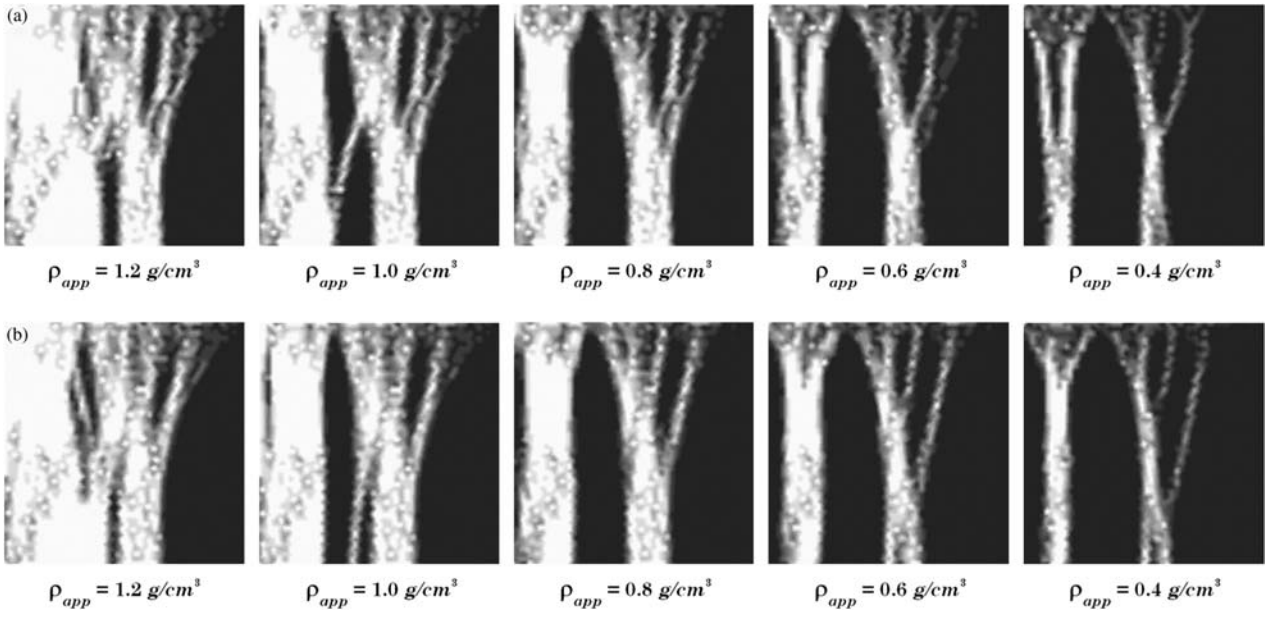


Figure 4. Evolution of the trabecular architecture in the square bone patch considering the proposed anisotropic material law (a) and Lotz anisotropic material law (b).

with a volume $2 \times 1 \times 2\,\text{mm}^3$. A surface load $F = 1.0\text{N}/\text{mm}^2$, with the direction indicated in the figure, is applied in two square areas on the top of the hexahedron patch. On the patch bottom, another two square areas locally constrain the patch movement in all directions. The problem is analysed considering the regular mesh, with 2681 nodes, presented in Figure 6(c). To present the results, the cubic patch is cut by the section presented in Figure 6(d).

In this example, only the new proposed material law is considered in the bone remodelling algorithm. For all studied examples, a uniformly initial density distribution $\rho_{\text{app}}^{\max} = 2.1\text{g}/\text{cm}^3$ is assumed for the three-dimensional patch, with a Poisson ration $\upsilon = 0.3$, regardless of the material direction.

The evolution of the trabecular bone remodelling process is presented in Figure 7(a). As expected, the applied loads lead the bone to build vertical trabeculae.

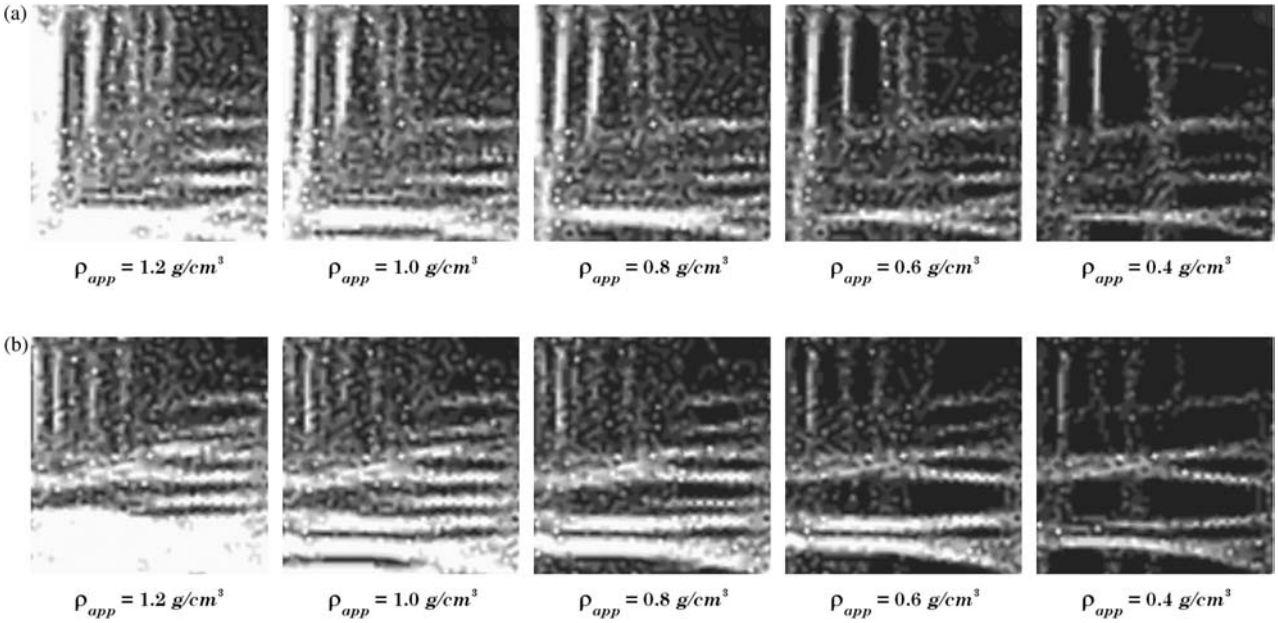


Figure 5. Evolution of the trabecular architecture in the square bone patch for the two load cases: L1 with 1000 cycles and L2 with 1000 cycles (a) and considering the two load cases: L1 with 1000 cycles and L2 with 5000 cycles (b).

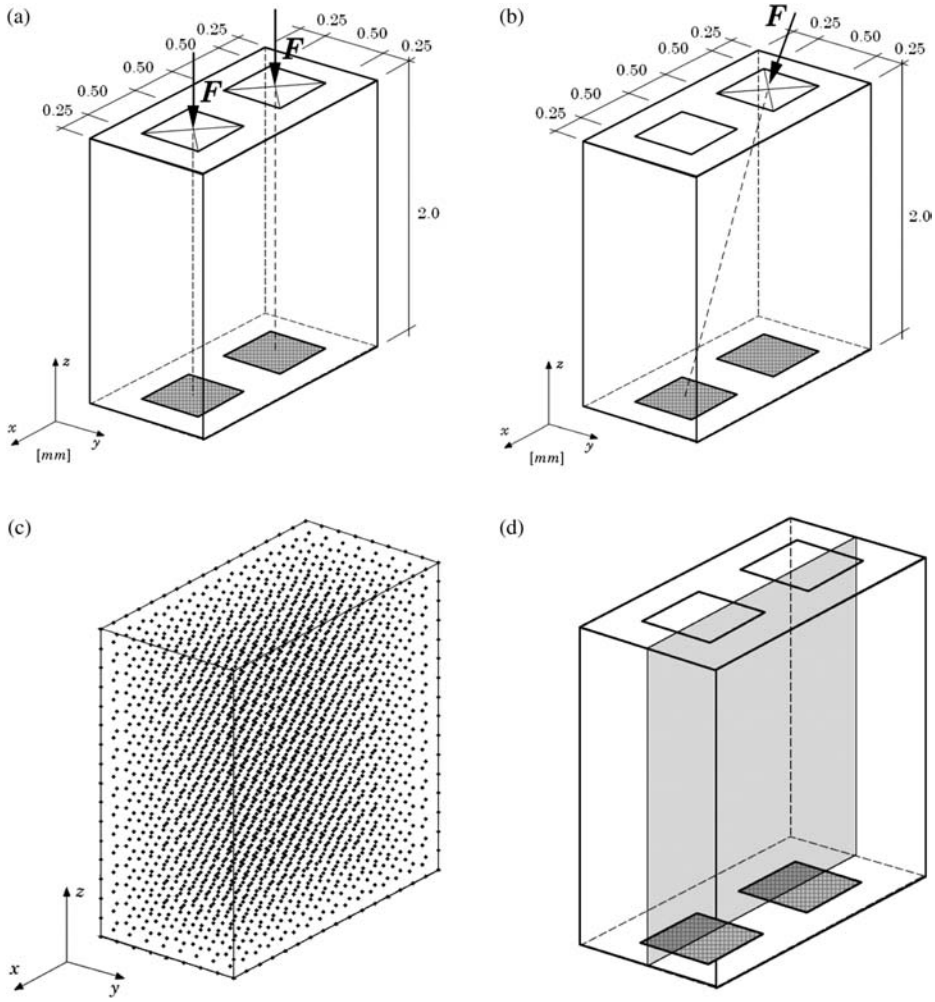


Figure 6. (a) Hexahedron bone patch model submitted to vertical loads; (b) hexahedron bone patch model submitted to a diagonal load; (c) regular nodal mesh (2681 nodes); (d) patch section cut.

To verify the influence of the nodal mesh discretisation, a single diagonal load is considered, as Figure 6(b) illustrates. The same essential boundary conditions and material properties are assumed. The results are presented in Figure 7(b). It is visible that evolution of the trabecular bone remodelling process leads to a single diagonal trabecula. The three-dimensional section views for both analyses are presented in Figure 7(c), when the apparent medium density $\rho_{app} = 0.4\text{g/cm}^3$ is achieved. Note that, as expected, the bone seams to form cylindrical trabeculae in the direction of the applied load.

Another hexahedron example is studied. Consider the cubic patch presented in Figure 8(a), with dimensions $2 \times 2 \times 2\,\text{mm}^3$. A surface load $F = 1.0\text{N/mm}^2$, with the direction indicated in the figure, is diagonally applied in a square area on the top of the cubic patch. On the patch bottom, four square areas locally constrain the patch movement in all directions. The problem is analysed considering a regular mesh with 2744 nodes (Figure 8(b)). The same material properties are assumed as in the previous example. To present the results, the cubic patch is cut by the section presented in Figure 8(c). The results regarding the evolution of the trabecular bone remodelling process are presented in Figure 9. Further, despite the applied load being not collinear with the mesh distribution, the formed trabecula is perfectly oriented in the load direction. Note that for apparent density $\rho_{app} > 0.6\text{g/cm}^3$ a secondary trabecula remains in the bone patch. The structural function of this secondary trabecula is to stabilise the principal diagonal trabecula, stopping a possible buckling phenomenon. The manifestation of the secondary trabecula proves that the remodelling algorithm and the proposed material law can predict also for the three-dimensional analysis secondary structures in the trabecular bone medium.

To end this section dedicated to the three-dimensional bone patch analysis, the same cubic bone patch with $2 \times 2 \times 2\,\text{mm}^3$ is analysed; however, in this case surface loads $F = 1.0\text{N/mm}^2$ are cross-diagonally applied in

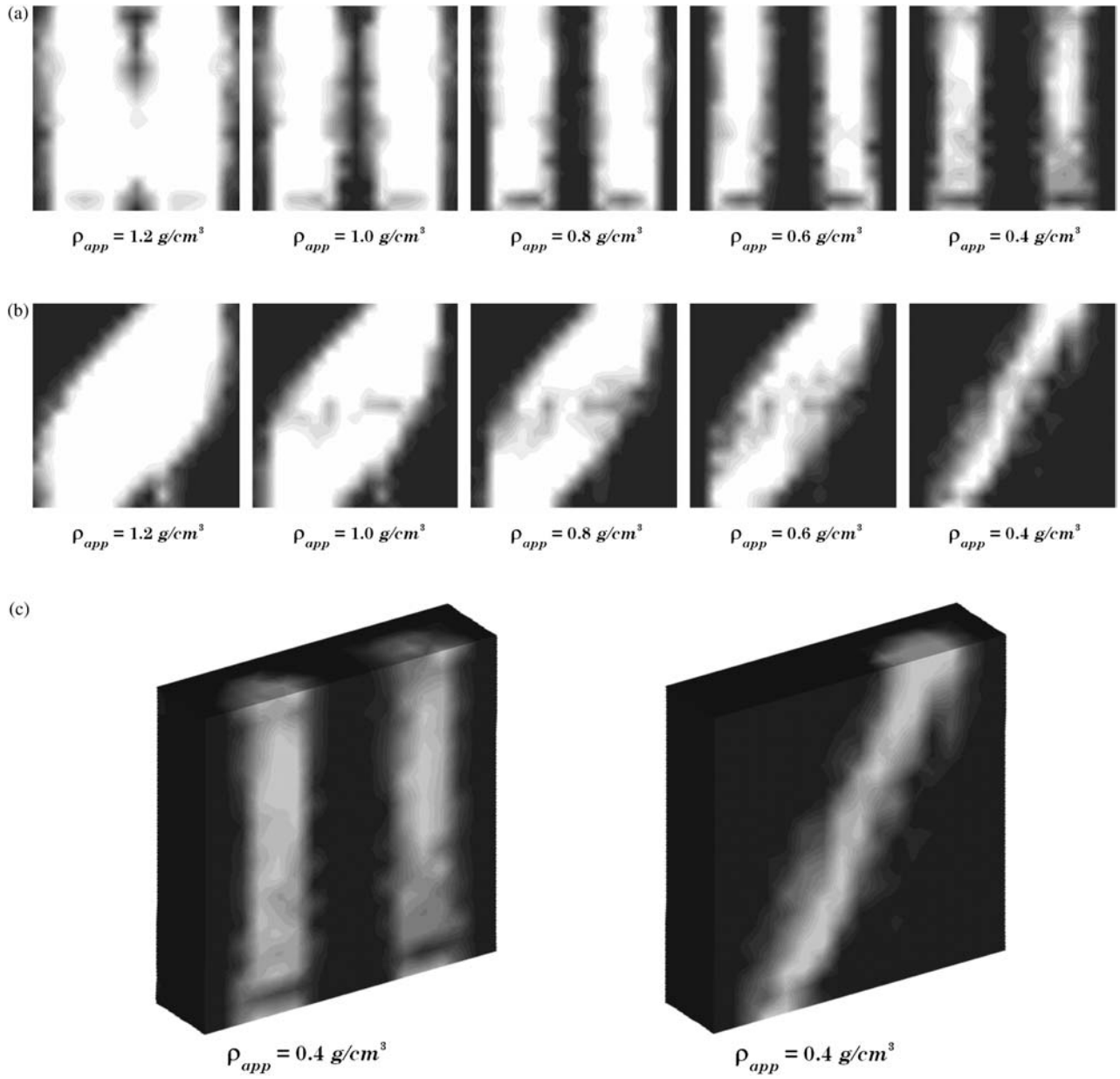


Figure 7. Evolution of the trabecular architecture in the bone hexahedron patch (a) for vertical loads, (b) for diagonal load, and (c) three-dimensional view.

square areas on the top of the cubic patch (Figure 10(a)). The essential boundary conditions are the same as in the previous analysis; the bottom four square areas locally constrain the cubic patch movement in all directions. The problem is analysed considering the same regular mesh presented in Figure 8(b). With this example, it is expected to stimulate the torsion effects in the bone patch; in response the bone must resist remodelling into suitable trabecular structure. To observe the internal bone reorganisation, four cut sections are made in the cubic patch (Figure 10(b)).

The present analysis was performed using three bone tissue material laws. First, the cubic bone patch was analysed considering the bone as an isotropic material. This governing mathematical law was obtained from the new anisotropic material law proposed in this work, considering for the transverse direction the correspondent axial values to respect the isotropic material assumption. The results on the evolution of the medium apparent density in the bone cubic patch for the cross-load are presented in Figure 11. The results of Figure 11 show that the bone forms standardised diagonal trabeculae to resist the torsion effect produced by the applied load. Secondary trabeculae do not appear as evident structures. Therefore, the study continues and the cubic patch was analysed considering the bone as

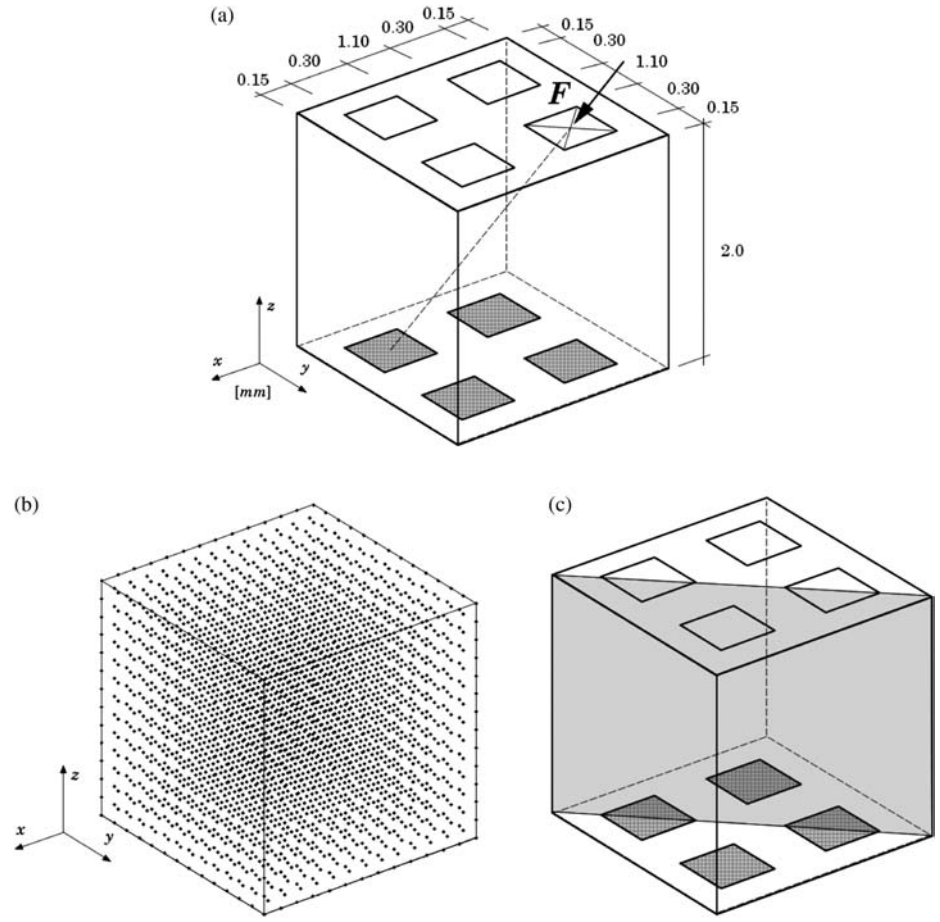


Figure 8. (a) Cubic patch model submitted to a diagonal load; (b) regular nodal mesh (2744 nodes); (c) patch section cut.

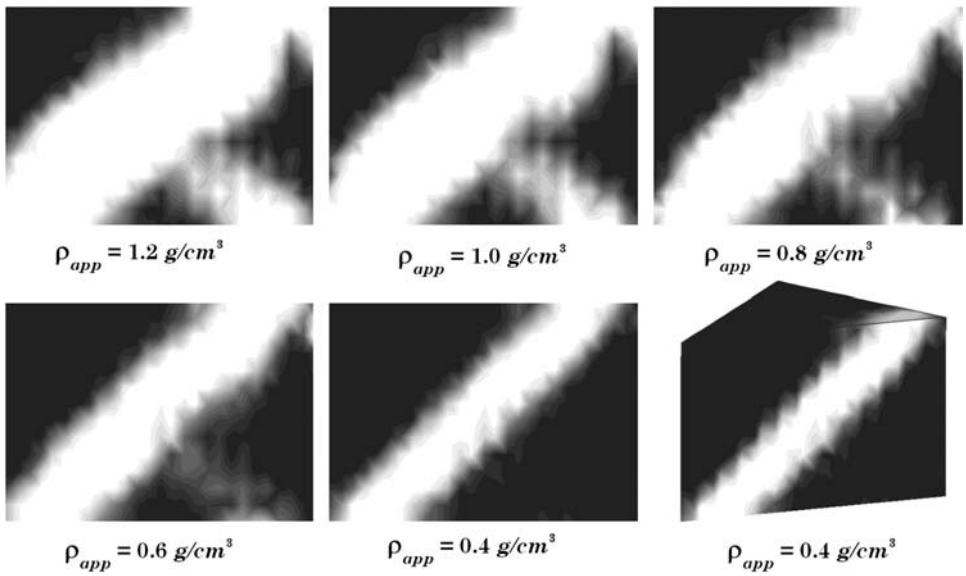


Figure 9. Evolution of the trabecular architecture in the bone cubic patch for diagonal load.

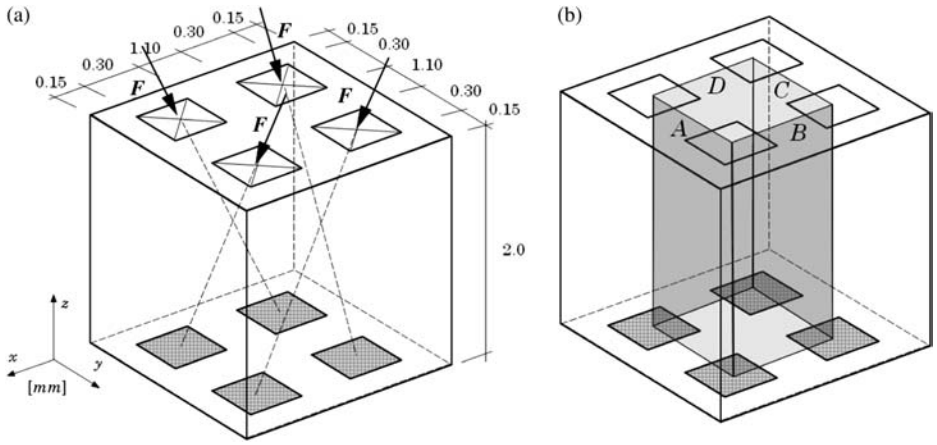


Figure 10. (a) Cubic patch model submitted to cross-diagonal loads; (b) patch sections cuts.

an anisotropic material, fully using the material law proposed in this work. The results are shown in Figure 12 and it is possible to observe the growth of secondary trabecular structures in the vertical direction. These results are corroborated with the solution obtained when the Lotz et al.'s anisotropic material law is considered (Figure 13). The same vertical secondary structures appear when the Lotz et al.'s anisotropic material law is considered. This example proved that in the bone trabecular remodelling process it is important to consider the bone as an anisotropic material. The secondary trabecular structures confer to the trabecular bone mesh a higher stability and resistance. The manifestation of such structures indicates that the present study on bone remodelling is moving forward in a right path.

### 3.3. *Extention to the macroscale analysis*

The femur bone is probably the most studied bone example available in the literature (Beaupré et al. 1990a,b; Jacobs et al. 1997, Doblaré and García 2002; Jang and Kim 2010). Considering the meshless approach, the most relevant work available in the literature regarding the remodelling analysis is probably the work of Doblaré et al. (2005). The femur bone loading history is approximated by the three-load cases used by Beaupré et al. (1990a,b), each consisting of one parabolic distributed load over the joint surface and another parabolic distributed load on the trochanter, representing the abductor muscle attachment.

In this study, a two-dimensional model of the femur is analysed. The femoral model is discretised with an irregular mesh of 5991 nodes and the three-load cases proposed by Beaupré et al. (1990a,b) are applied with the correspondent magnitude. The remodelling algorithm proposed in this work is applied combined with the new anisotropic material law proposed. The femoral macroscale analysis results for a medium apparent density of $\rho_{app} > 1.2 g/cm^2$ are presented in Figure 14. Note that it is possible to observe the internal trabecular structures indicated in the X-ray plate shown in Figure 3(a) and the remaining internal formations such as the Ward's triangle and the greater trochanteric group. Note that the secondary structures can also be accurately predicted with the proposed remodelling algorithm and bone anisotropic material law.

## 4. Conclusions and final remarks

In the present work, a novel anisotropic material law for the mechanical behaviour of the bone tissue is proposed, along with a new gradient remodelling algorithm that considers an improved meshless method for the strain and stress evaluation. The proposed bone tissue anisotropic material law is based on experimental data available in the literature and permits to correlate accurately the bone density with the obtained level of stress by means of a mechanical stimulus. The proposed bone tissue remodelling algorithm imposes a gradient transition from the initial isotropic cortical assumption to the final anisotropic trabecular arrangement.

The proposed model is simple to apply and depends mainly on the SED field, which is obtained multiplying the stress field by the strain field for each interest point (integration point). It was shown in the previous works (Dinis et al. 2007, 2008, 2009, 2010) that the NNRPIM is more accurate than other meshless methods and the FEM, and produces smoother strain and stress fields. Therefore, the inclusion of the NNRPIM in the remodelling analysis is an asset and not just another way to obtain the SED field. The accuracy of the remodelling algorithm depends on the accuracy of the used numerical method.

It was verified that the introduction of the proposed new bone tissue anisotropic material law reduces the number of iterations and increases the quality of the results. The reduction of the number of iterations is explained with the

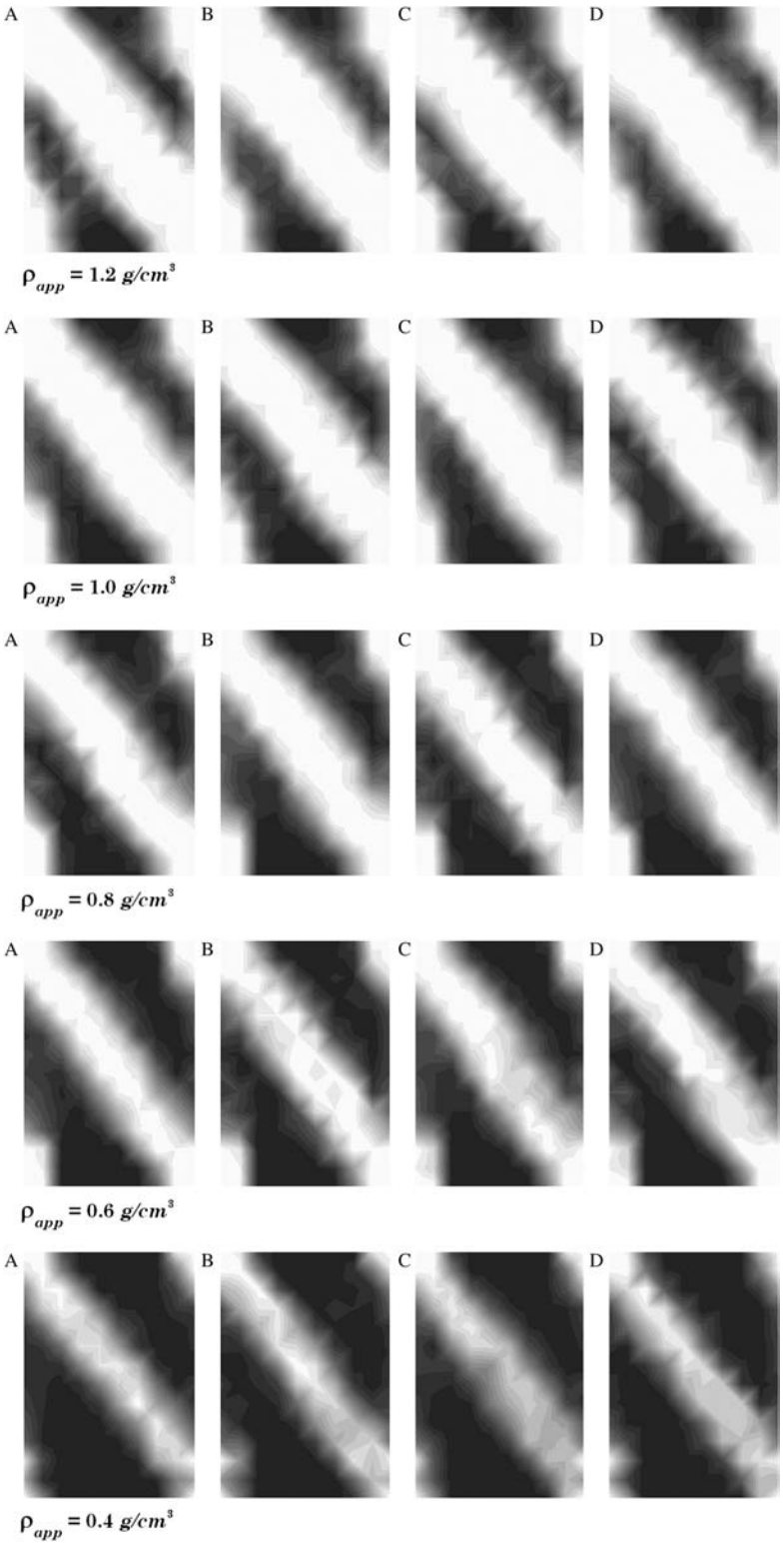


Figure 11. Evolution of the trabecular architecture in the bone cubic patch for the cross-diagonal loads (isotropic material considering the proposed material law).

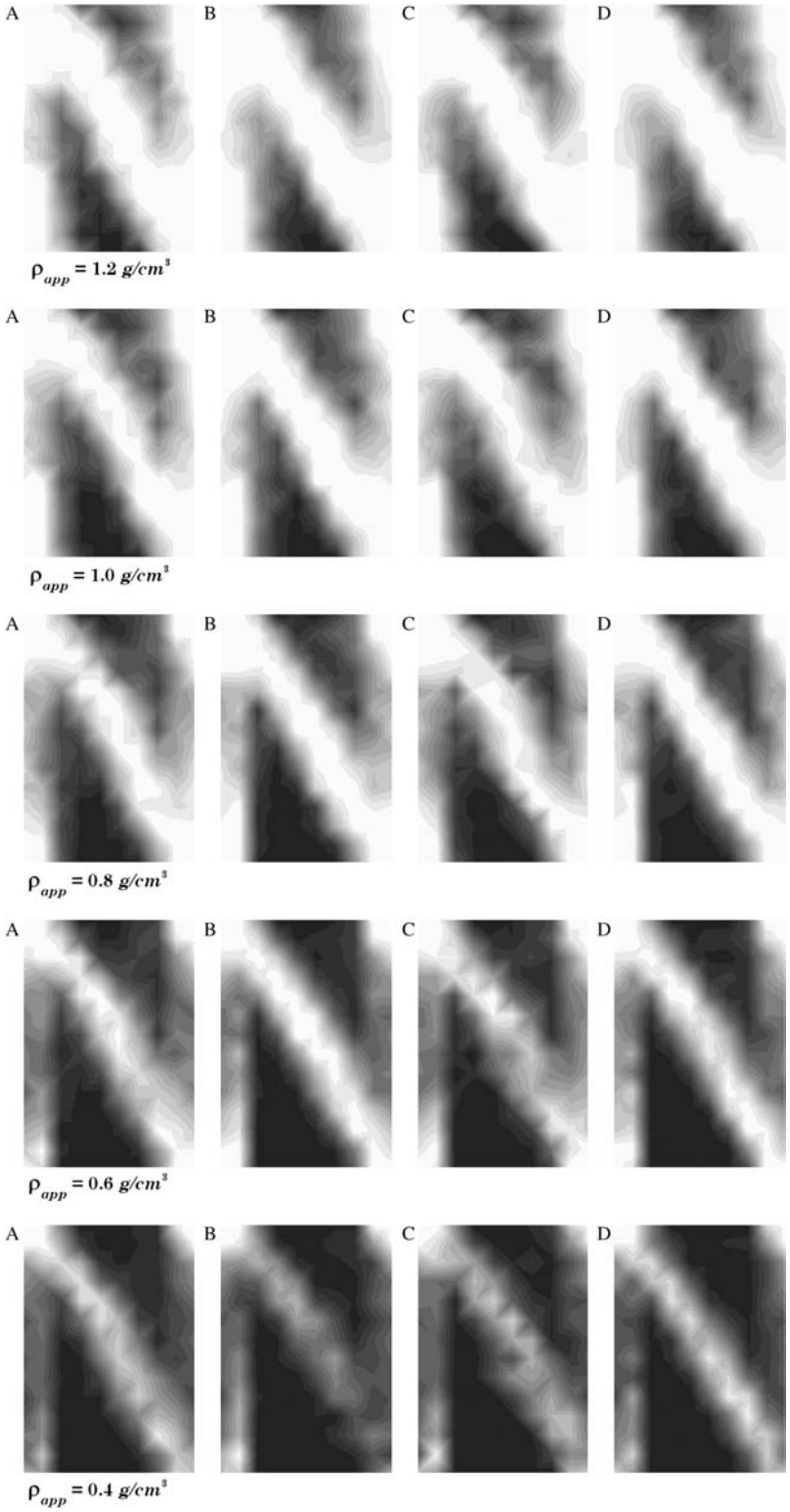


Figure 12. Evolution of the trabecular architecture in the bone cubic patch for the cross-diagonal loads (anisotropic material considering the proposed material law).

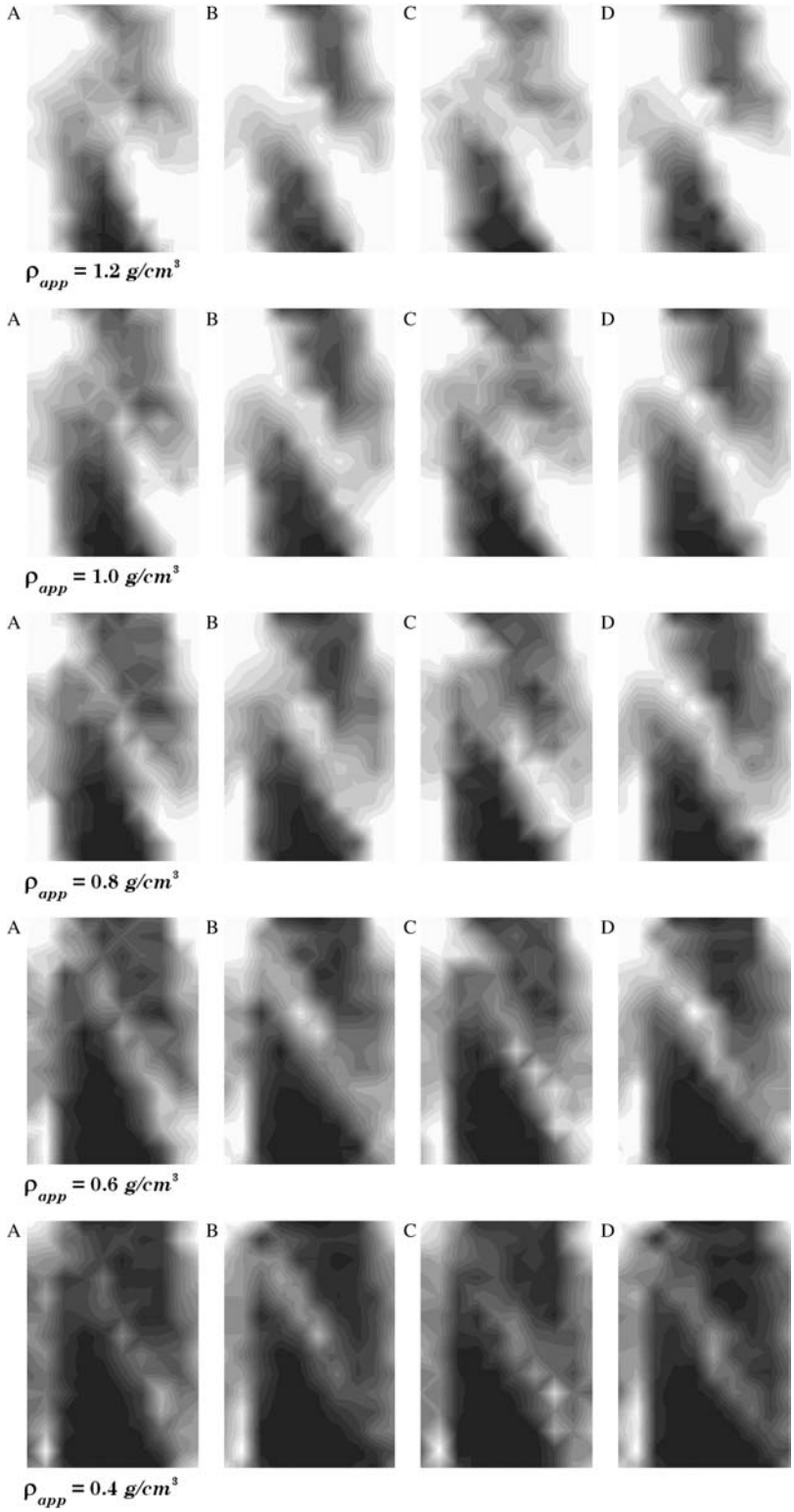


Figure 13. Evolution of the trabecular architecture in the bone cubic patch for the cross-diagonal loads (anisotropic material considering Lotz material law).

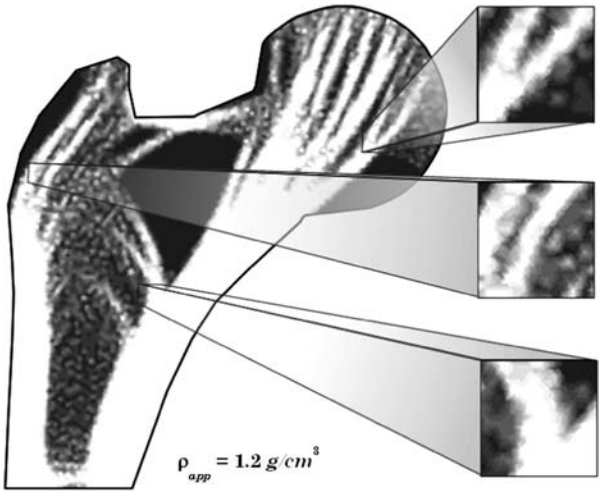


Figure 14. Trabecular architecture in the femoral bone when the three mechanical cases are applied simultaneously.

difference between the material curve tangential slopes in the bone cortical state and the bone trabecular state (Figure 1). The quality of the results is explained with the origin of the proposed material law: an exhaustive and complete experimental work performed by Zioupos et al. (2008) on various bone tissue micropatches.

It is visible that for the same medium patch density the results obtained with the proposed material law (Figure 12) are consistently more defined (the trabecular contour is always more delineated) than the ones presented in Figure 13, which is obtained considering Lotz et al.'s material law. This indicates that the proposed anisotropic bone tissue material law permits a more defined trabecular arrangement.

Several examples well documented in the literature were studied and solved, and the following conclusions may be established. The proposed bone anisotropic material law permits a smooth transition between the cortical bone stage and the trabecular bone condition, which can be observed in the totality of the presented analysis. The level of the domain discretisation plays an important role in the analysis. However, even for more course meshes the remodelling algorithm is able to predict accurately the major internal bone trabecular structures. The proposed bone tissue remodelling algorithm combined with the NNRPIM accuracy permits to predict correctly the secondary trabecular structures, which are very important in the stability of the principal structures.

For the time being, the great disadvantage of using the NNRPIM in the bone tissue remodelling analysis is the considerable computational cost for the three-dimensional analysis combined with the need of a very large cloud of nodes to obtain a good definition of the trabecular structure.

The developed work and the obtained results permit to conclude that the presented gradient remodelling algorithm, combined with the proposed anisotropic material law and the meshless method, has the potential to improve future numerical incursions on the bone regeneration procedure after fracture and the osseointegration process.

## Acknowledgements

The authors truly acknowledge the funding provided by Ministério da Ciência, Tecnologia e Ensino Superior – Fundação para a Ciência e a Tecnologia (Portugal), under grant SFRH/BPD/75072/2010, and by FEDER/FSE, under grant PTDC/EME-TME/098050/2008.

## Notes

1. **Email: rnatal@fe.up.pt
2. †Email: ldinis@fe.up.p

## References

Beaupré GS, Orr TE, Carter DR. 1990a. An approach for timedependent bone modelling and remodelling; theoretical development. J Orthop Res. 8(5):651–661.

Beaupré GS, Orr TE, Carter DR. 1990b. An approach for timedependent bone modelling and remodelling: a preliminary remodelling simulation. J Orthop Res. 8(5):662–670.

Carter DR, Fyhrie DP, Whalen RT. 1987. Trabecular bone density and loading history: regulation of connective tissue biology by mechanical energy. J Biomech. 20(8):785–794.

Carter DR, Hayes WC. 1977. The compressive behavior of bone as a two phase porous structure. J Bone Joint Surg. 59(A):954–962.

Carter DR, Orr TE, Fyhrie DP. 1989. Relationship between loadingt history and femoral cancellous bone architecture. J Biomech. 22(3):231–244.

Carter DR, Spengler DM. 1978. Mechanical properties and composition of cortical bone. Clin Orthop Relat Res. 135:192–217.

Cowin SC, Hegedus DH. 1976. Bone remodeling I: a theory of adaptive elasticity. J Elast. 6:313–326.

Dinis LMJS, Jorge RMN, Belinha J. 2007. Analysis of 3D solids using the natural neighbour radial point interpolation method. Comput Methods Appl Mech Eng. 196(13–16):2009–2028.

Dinis LMJS, Jorge RMN, Belinha J. 2008. Analysis of plates and laminates using the natural neighbour radial point interpolation method. Eng Anal Boundary Elem. 32(3):267–279.

Dinis LMJS, Jorge RMN, Belinha J. 2009. Large deformation applications with the radial natural neighbours interpolators. Comput Modell Eng Sci. 44(1):1–34.

Dinis LMJS, Jorge RMN, Belinha J. 2010. shell-like approach using a natural neighbour meshless method: isotropic and orthotropic thin structures. Compos Struct. 92(5):1132–1142.

Doblaré M et al., 2005. On the employ of meshless methods in biomechanics. Comput Methods Appl Mech Eng. 194:801–821.

Doblaré M, García JM. 2002. Anisotropic bone remodelling model based on a continuum damage-repair theory. J Biomech. 35(1):1–17.

Gibson LJ. 1985. The mechanical behaviour of cancellous bone. J Biomech. 18:317–328.

Goldstein SA. 1987. The mechanical properties of trabecular bone: dependence on anatomic location and function. J Biomech. 20:1055–1061.

Jacobs CR et al., 1997. Adaptive bone remodeling incorporating simultaneous density and anisotropy considerations. J Biomech. 30(6):603–613.

Jang IG, Kim IY. 2010. Computational simulation of simultaneous cortical and trabecular bone change in human proximal femur during bone remodeling. J Biomech. 43:294–301.

Keyak JH, Rossi SA. 2000. Prediction of femoral fracture load using finite element models: an examination of stress- and strain-based failure theories. J Biomech. 33(2):209–214.

Lotz JC, Gerhart TN, Hayes WC. 1991. Mechanical properties of metaphyseal bone in the proximal femur. J Biomech. 24(5):317–329.

Martin RB. 1991. Determinants of the mechanical properties of bones. J Biomech. 24(1):79–88.

Mullender MG, Huiskes R, Weinans H. 1994. A physiological approach to the simulation of bone remodeling as a selforganizational control process. J Biomech. 27(11):1389–1394.

Nguyen VP et al., 2008. Meshless methods: a review and computer implementation aspects. Math Comput Simul. 79(3):763–813.

Reilly DT, Burstein AH. 1975. The elastic and ultimate properties of compact bone tissue. J Biomech. 8(6):393–405.

Rice JC, Cowin SC, Bowman JA. 1988. On the dependence of the elasticity and strength of cancellous bone on apparent density. J Biomech. 21(2):155–168.

Sansalone V et al., 1857. Determination of the heterogeneous anisotropic elastic properties of human femoral bone: from nanoscopic to organ scale. J Biomech. 43–1863.

Shefelbine SJ et al., 2005. Trabecular bone fracture healing simulation with finite element analysis andfuzzy logic. J Biomech. 38:2440–2450.

Weinans H, Huiskes R, Grootenboer HJ. 1992. The behaviour of adaptive bone-remodelling simulation models. J Biomech. 25(12):1425–1441.

Wirtz DC et al., 2000. Critical evaluation of known bone material properties to realize anisotropic FE-simulation of the proximal femur. J Biomech. 33:1325–1330.

Wolff J. 1986. The law of bone remodeling [Das Gesetzder Transformationder Knochen]. Berlin/Heidelberg/New York: Springer.

Xinghua Z et al., 2002. A study of the effect of non-linearities in the equation of bone remodeling. J Biomech. 35:951–960.

Zioupos P, Cook RB, Hutchinsonc JR. 1961. Some basic relationships between density values in cancellous and cortical bone. J Biomech. 41–1968.